Carbon 215 (2023) 118424

Contents lists available at ScienceDirect

Carbon

journal homepage: www.elsevier.com/locate/carbon

Achieving superlubricity and high adhesion strength of hydrogenated amorphous carbon film with Al/Cr/Si-doping

Quansheng Ma [a], Yongqiang Fu [a,c,**], Yi Xu [b,***], Tianbao Ma [a,*]

[a] State Key Laboratory of Tribology in Advanced Equipment, Tsinghua University, Beijing, 100084, China
[b] Institute of Mechanics, Chinese Academy of Sciences, Beijing, 100190, China
[c] School of Mechanical and Automotive Engineering, Qingdao University of Technology, Qingdao, 266520, China

ARTICLE INFO

Keywords:
AlCrSi/a-C:H
Co-doping
Superlubricity
Adhesion strength

ABSTRACT

Excellent tribological properties of hydrogenated amorphous carbon films make it an important candidate for friction reduction in industry. However, the great challenge of achieving both high adhesion strength and super-low friction limits its wide applications. In this work, a novel Al, Cr and Si co-doped hydrogenated amorphous carbon (AlCrSi/a-C:H) film was prepared by high-power impulse magnetron sputtering (HiPIMS) method. The AlCrSi/a-C:H film showed favorable mechanical performance and high adhesion (~80 N), which was attributed to the controlled elements doping and special transition layers produced by HiPIMS method. Meanwhile, superlubricity was obtained with coefficient of friction 0.0014. Detailed characterizations suggested that doping elements played significant roles in tribo-chemical reactions during friction. On one hand, doping elements can promote shear-induced graphitization and formation of graphite-like layers at the friction interface. On the other hand, the preferential oxidation of doping elements can protect the formed graphite-like layers from oxidation and the formed oxides nanoparticles can also be wrapped by carbon layers to prevent abrasive wear. It was the synergistic effects of graphitization and oxidation actions that led to superlubricity state of the film. The proposed AlCrSi/a-C:H film architecture with strong adhesion and superlubricity properties provides design criteria of superlubricious films for industrial applications.

1. Introduction

Extreme conditions involving vacuum and cryogenic environment bring huge challenges to the lubrication of friction pairs like bearings, gears, and valves [1–4]. Solid lubricants are gradually widely used because of their excellent stability and chemical inertness compared with oil and grease under these extreme conditions. Hydrogenated amorphous carbon (a-C:H) film is an alternative candidate due to its low coefficient of friction (COF) and unique mechanical properties [2,5–9]. Up to now, it has been widely reported that a-C:H film can achieve superlubricity (COF <0.01) in certain conditions [10–19]. However, it is still subject to various adverse factors, especially the humid atmosphere due to the tribo-oxidation reaction of oxygen/water-molecules and carbon across the slip interface [12,20–22]. Beyond that, the high internal stress in a-C:H film also deteriorated the adhesion strength with substrate.

Although important progresses [23–32] have been made during past decades, achieving both superlubricity and strong adhesion strength remains a challenge for the carbon-based films, which limited their industrial applications. To improve adhesion strength, it is necessary to relax the internal stress in the film and the addition of metallic elements into carbon matrix is an effective method [33–37]. Among them, Cr, Ti and Al elements have been proven by numerous studies [35,38–40] to effectively reduce the internal stress of a-C:H films. Meanwhile, the doping of Cr or Ti elements could improve the hardness of films due to the formation of hard carbide phases [41,42], and the doping of Al element could promote the formation of sp^2 clusters and reduce the friction coefficient (0.024–0.089) [43]. However, higher doping of metallic elements would also decrease the friction performance due to the reduction of carbon source required for graphitized carbon layers [44,45]. Additionally, the formation of hard metal carbide particles between Cr/Ti and C could result in abrasive wear [30,46], and the

* Corresponding author.
** Corresponding author.
*** Corresponding author.
E-mail addresses: yqfu@nuaa.edu.cn (Y. Fu), xuyi@imech.ac.cn (Y. Xu), mtb@mail.tsinghua.edu.cn (T. Ma).

https://doi.org/10.1016/j.carbon.2023.118424
Received 20 June 2023; Received in revised form 18 August 2023; Accepted 29 August 2023
Available online 29 August 2023

reduced hardness caused by higher Al elements content in carbon matrix would also decrease the wear resistance [31,47]. Furthermore, it has been reported that silicon, a non-metallic element, is a commonly used doping element to reduce the environment sensitivity of friction of a-C:H film and achieve superlubricity in humid air [48–50]. This is attributed to the formation of layered-like tribo-film by absorbing water molecules in the humid air [48]. In summary, although strong adhesion strength or superlubricity of carbon film has been achieved by single or dual element doping [31,46,51], there are few reports on simultaneously achieving strong adhesion and superlubricity strength up to now.

Consequently, aiming to optimize the tribological performances while ensuring the good adhesion of the a-C:H films, we reported the a-C:H nanocomposite film with Al, Cr and Si multi-doping (AlCrSi/a-C:H). In our work, high-power impulse magnetron sputtering method was applied to introduce the Al, Cr, and Si elements into a-C:H films. The phase characterizations were analyzed and the friction performances were studied systemically. The AlCrSi/a-C:H films with high adhesion strength achieved superlubricity, and the superlubricity mechanisms were elaborated with respect to the contact surfaces, transfer films and wear debris.

2. Experimental details

2.1. Materials

The synthetizations of Al, Cr and Si multi-doping a-C:H films on 9Cr18 stainless steel substrates were performed in a home-made PVD apparatus equipped with HiPIMS (HighPulse 4002, Huttinger Electronic) power supplies (Fig. 1). The HiPIMS technique with low frequency (< 10 kHz) and duty (< 10%) power was applied to the target in pulse leading to pulse target power densities of several kilowatt per square centimeter [52]. Therefore, the deposited films showed the low roughness, high density and crystallinity [53],and enables more direct control over the deposition process.

Before the deposition process, 9Cr18 stainless steel plates were polished to within 100 nm (Ra) of the surface roughness, and cleaned ultrasonically in acetone, ethanol, and deionized water for 20 min, respectively. After that, they were dried quickly by hot air and fixed on the base rod facing the target with a distance about 12 cm. When the base pressure was evacuated to the vacuum of 5×10^{-3} Pa, the substrates were cleaned using Ar ions sputtering with the applied −900 V bias voltage on substrates and 1.2 Pa pressure of the chamber for 20 min to remove oxides and contaminants. Prior to the deposition of AlCrSi/a-C:H films, the transition layers of AlCrSi, AlCrSiN were deposited to enhance films adhesion. Firstly, a high bias voltage of −800 V was used for 10 min (AlCrSi-I) to increase the ions bombardment energy in order to inject some target material ions into the subsurface of the steel. Afterwards, the bias voltage decreased to −100 V for 3 min to fabricated the AlCrSi layer (AlCrSi-II). Then 40 sccm N_2 was introduced to the chamber to deposited AlCrSiN layer for 3 min to improve mechanical properties of the films. After that, the flow of N_2 gradually reduced to 0 sccm from the initial 40 sccm, meanwhile the C_2H_2 gradually increased from 0 sccm to the final 50 sccm to eliminate the mechanical properties difference between the AlCrSiN and AlCrSi/a-C:H layers, and the whole process lasted for 5 min. Finally, the deposition of top layer (AlCrSi/a-C:H layer) lasted for 15 min. From the AlCrSiN layer to AlCrSi/a-C:H layer, the bias voltage and Ar flow were set as −100 V and 150 sccm, and the HiPIMS volage, pulse frequency and pulse time were kept 700 V, 200 Hz and 100 μs, respectively. The detail parameters of the film's deposition were listed in Table 1.

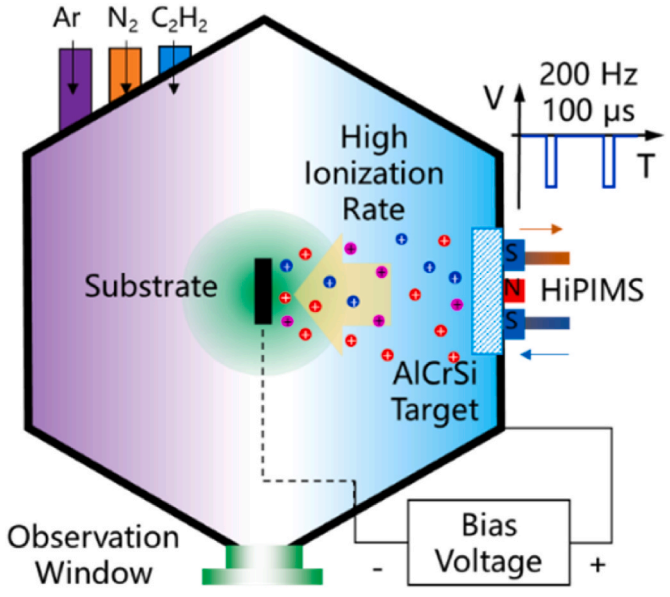

Fig. 1. Schematic diagram of HiPIMS deposition equipment. (A colour version of this figure can be viewed online.)

2.2. Characterizations

The structure morphology, thickness and elements distributions of the as-deposited films were analyzed by a high-resolution transmission electron microscope (HRTEM; JEOL JEM F200, Japan) equipped with an energy dispersive spectroscopy (EDS). The cross-sections of AlCrSi/a-C:H film and transfer film were prepared by the focus ion beam (FIB, FEI-Quanta 3D FEG) method. The atomic bond structures of the AlCrSi/a-C:H films before and after the friction tests were detected by the Raman spectroscopy (LabRAM HR Evolution, Horiba Scientific, wavelength of 532 nm). The chemical bonds of films before and after the friction tests were tested by the X-ray photoelectron spectroscope (XPS; PHI Quantera II, Japan). The phase structures of AlCrSi/a-C:H films were analyzed by the X-ray diffraction (XRD; Bruker, Germany) with the 2θ ranged from 5 to 90°. In order to further analyze the formation of transfer films, the morphologies and elements mapping distributions of the wear scars were detected by scanning electron microscope (SEM; Quanta 200 FEG, Netherlands). Besides, the transfer films and wear debris were characterized by SEM and TEM to study the superlubricity mechanism.

The nano-hardness and elastic modulus of the AlCrSi/a-C:H films were measured by the nanoindentation technique (NIT; CSM, Switzerland), and the indentation depth was set as 1/10 of the thickness (300 nm) of AlCrSi/a-C:H films, to avoid the influence of substrate and transition layers. The adhesion force was tested by a scratch tester (WS-2005, Scratch tester, China), and the acoustic emission signals were also collected during the whole testing process and the maximum load was 80 N. The morphologies of wear tracks, wear scars, Vickers hardness indentation and scratch were observed by optical microscope (Keyence, VHX-100X, Japan).

2.3. Friction and wear

The friction and wear tests were conducted using the rotational ball-

Table 1
Parameters of film's deposition.

Deposition process	Flow rate (sccm)			Bias voltage (V)	HiPIMS	Time (min)
	Ar	N_2	C_2H_2			
AlCrSi-I	150	/	/	−800	Voltage:	10
AlCrSi-II		/	/	−100	700V	3
AlCrSiN		40	/		Pulse	3
AlCrSiCN		40 → 0	0 → 50		frequency: 200 Hz	5
AlCrSi/a-C:H		/	50		Pulse time: 100 μs	15

on-disc tribometer (MMQ-02L, Jinan Yihua tribology testing technology Co.,LTD, China) at room temperature. The tests were repeated three times under each operating condition, and the average value was taken as the final data. Two friction pairs were used: (1) AlCrSi/a-C:H plate against the bare 9Cr18 stainless steel ball (bare-ball); (2) AlCrSi/a-C:H plate against the ball with a-C:H film (a-C:H-ball). And they were performed in two kinds of environments: (1) low humidity (RH: 7 ± 1%) (hereinafter referred to as RH-7%), realized by feeding nitrogen into the relatively closed friction chamber; (2) the open air with high humidity (RH: 52 ± 2%) (hereinafter referred to as RH-52%). The diameter of mating ball was 6 mm. The applied load was 8 N (Hertzian contact pressure: 1.3 GPa), and rotation speed was 100 rpm (rotational radius: 10 mm, linear speed: 0.21 m/s). The wear volumes of films were calculated by the cross-sectional profiles of wear track, which measured using a non-contact three-dimensional white light interferometer (Nex view, ZYGO Lamda, USA), and the wear rates were calculated by Archard equation [54]: Wear rate (mm^3/N·m) = Wear volume (mm^3)/(Applied load (N) × Sliding distance (m)).

3. Results and discussion

3.1. Characterizations of the original AlCrSi/a-C:H film

Fig. 2a showed the cross-sectional construction of AlCrSi/a-C:H film characterized by the low-magnification TEM. The whole film included five layers obviously, AlCrSi-I, AlCrSi-II, AlCrSiN, AlCrSiCN and AlCrSi/a-C:H, and the thickness of these layers were 550 nm, 180 nm, 180 nm, 350 nm, and 1400 nm, respectively. The EDS-elemental line distributions of C, Al, Cr, Si, N, O, Fe and Pt along the white line were detected, and the element compositions of C, Al, Cr and Si in the AlCrSi/a-C:H area were 88.2%, 7.01%, 2.51% and 2.28%, respectively. Meanwhile, EDS-elemental mapping distributions of C, Al, Cr, Si, N, O, Fe and Pt as marked in Fig. 2a were also investigated (Fig. 2b), and the results were consistent with the line distributions. HRTEM image of the AlCrSi/a-C:H film showed the typical amorphous phase, and the corresponding selected area electron diffraction (SAED) pattern presented no diffraction ring which proved that the AlCrSi/a-C:H films mainly composed of amorphous phase (Fig. 2c). It was worth noting that some short, orderly coiled chain structures were found in the amorphous phase, which was a sign of the higher sp^2 content.

Raman spectroscopy was employed to confirm the atomic bond structure of the AlCrSi/a-C:H film, and the results showed that a broad asymmetric peak in the wavenumber around 1500 cm^{-1} in Fig. 2d, which was fitted into two Gaussian peaks at 1350 cm^{-1} and 1580 cm^{-1}, and they were assigned for the D band and G band, respectively [55–57]. The D band corresponds to the breathing modes of sp^2-C atoms in aromatic rings, and the G band corresponds to the bond stretching modes of sp^2-C atoms including both chains and aromatic rings [55–57]. The calculated I_D/I_G of 1.58 was a higher value compared with other references [16,58], which was also an indication of the increase of sp^2 clusters content and it was consistent with the results of HRTEM mentioned above. According to other studies [59,60], as the main

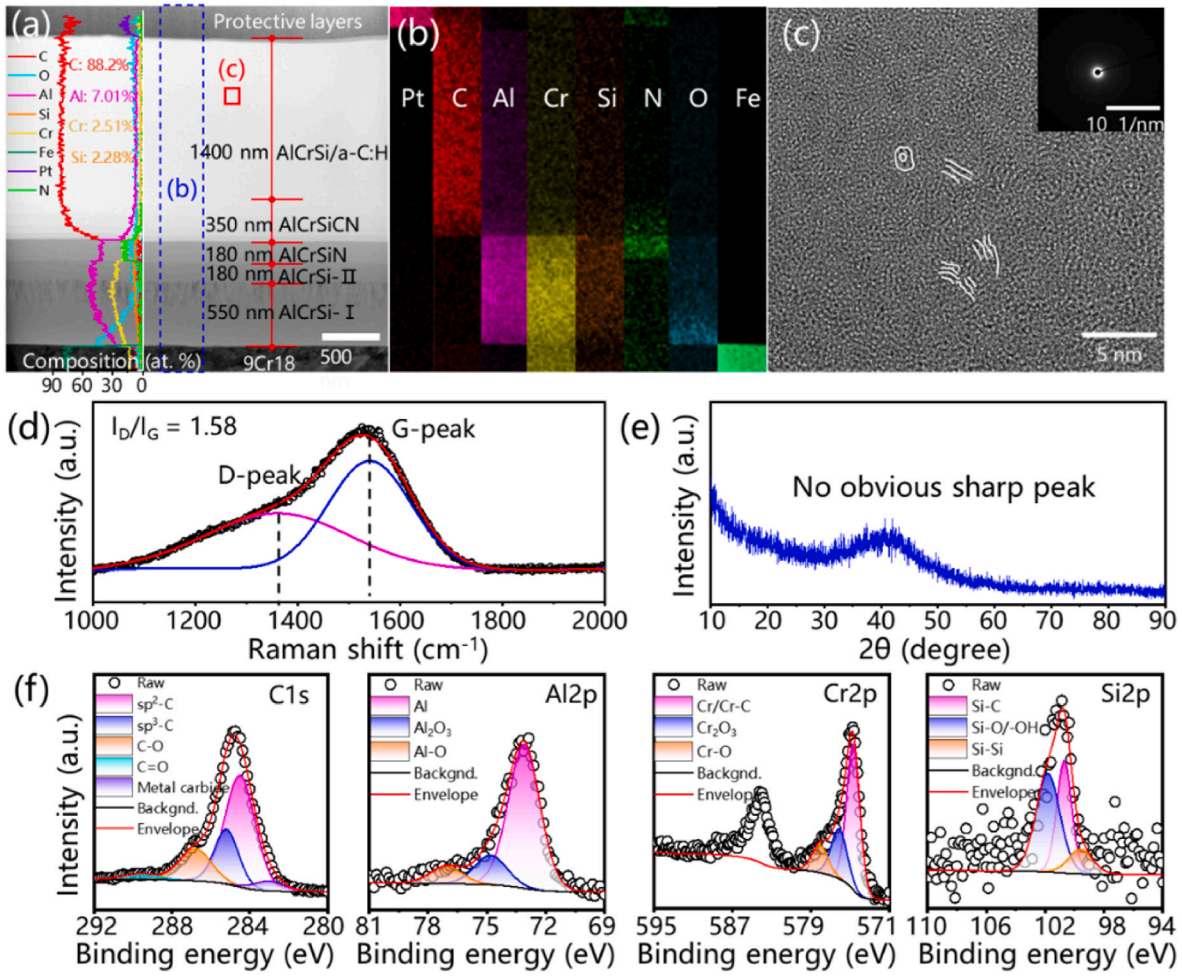

Fig. 2. Characterizations of original AlCrSi/a-C:H film: (a) TEM cross-sectional morphology and EDS-elemental line distributions of AlCrSi/a-C:H film. (b) EDS-elemental mapping distributions of AlCrSi/a-C:H film and (c) HRTEM image of AlCrSi/a-C:H film and the corresponding SAED pattern, as marked in (a). (d) Raman spectrum, (e) XRD results and (f) XPS spectra of original AlCrSi/a-C:H film. (A colour version of this figure can be viewed online.)

doping element, aluminum mainly contributed to the increase of sp^2 content. Additionally, the XRD spectrum of the AlCrSi/a-C:H film with a broad peak around 42° indicated that the AlCrSi/a-C:H film mainly composed of amorphous carbon phases without the signal of crystal phases (Fig. 2e). This result was in accordance with that of previous TEM analysis.

To further investigate the chemical bonds and elements concentration, survey scanning XPS spectrum for original AlCrSi/a-C:H film was observed (Fig. S1), which showed the mainly C1s, Al2p, Al2s, Cr2p, Cr3p, Si2p, Si2s and O1s peaks. To get the chemical bonds information of AlCrSi/a-C:H film, high-resolution XPS spectra of C1s, Al2p, Cr2p and Si2p peaks and the corresponding fits bands were detected as shown in Fig. 2f. As for C1s peak, it can be deconvoluted into five Gaussian peaks at 284.5 eV, 285.2 eV, 283 eV, 286.8 eV and 289.6 eV, which were typically assigned for sp^2-C, sp^3-C, metal carbides, C–O and C═O [61–63]. The Al2p peak was fitted into three peaks located at 73.11 eV, 74.81 eV and 77.09 eV, which were corresponding to the metallic Al, Al_2O_3 and other oxides of Al [46,64], and the fraction of metallic Al was up to 75.2%. Thus, it proved that the Al element mainly existed as the metallic state. For Cr2p peak, it was deconvoluted into three peaks: the main peak at 574.7 eV corresponding to the metallic Cr or Cr–C with its 61% fraction, and other two peaks 576.13 eV and 578.1 eV corresponding to the Cr–O in different valences [64,65]. Si2p spectrum was also fitted into three peaks located at 99.6 eV (Si–Si), 100.7 eV (Si–C) and 101.8 eV (Si–O/OH), in which the Si–C and Si–O/OH were two main bond types accounting for 36.2% and 51% [66]. From the XPS analysis of as-deposited AlCrSi/a-C:H film, it was clear that doping element mainly existed as the metallic state or the carbides rather than the oxides.

3.2. Mechanical properties of AlCrSi/a-C:H film

Furthermore, the mechanical properties of AlCrSi/a-C:H film were evaluated by nanoindentation technique, and the indentation force-depth curve was shown in Fig. 3a. The relevant data of nano-hardness (H), elastic modulus (E), H/E (the fracture toughness of the films) [67], H^3/E^2 (plastic deformation resistance of the films) [67] and elastic recovery were 12.3 ± 0.8 GPa, 115.2 ± 5.0 GPa, 0.107, 0.141 GPa and 65%, respectively. Due to the addition of aluminum, although the nano-hardness and elastic modulus were slightly lower, H/E and H^3/E^2 were relatively high, which implied good mechanical properties for AlCrSi/a-C:H films compared with other Al-containing a-C:H films [43,68,69], and it was most likely due to the addition of Cr elements [64,68].

To assess the adhesion strength of the film, the scratch test on the AlCrSi/a-C:H film surface was conducted, and the optical microscope image of scratch was showed in Fig. 3b. According to the scratch test method standard (ASTMC1624-2005) [70], the critical scratch load L_{C1} and L_{C2} were defined for cohesive cracking/failure in the film and subsequent adhesive failure/spalling between the film and the substrate at a higher applied normal force, respectively [71,72]. Usually, L_{C1} is associated with the start of chevron cracking, and L_{C2} with the start of chipping failure extending from the arc tensile cracks. According to Fig. 3b1 image, the L_{C1} was about 60 N, where the microcracks appeared. And there was still no spalling of film until the critical load increased to 80 N (Fig. 3b2), which indicated the good adhesion strength (L_{C2}: ~80 N) between the AlCrSi/a-C:H film and 9Cr18 stainless steel substrate.

To disclose the mechanism of strong adhesion force between the AlCrSi/a-C:H film and substrate, TEM and HRTEM characterizations of the AlCrSi/a-C:H film's interlayers were proformed. In Fig. 3c, TEM image and corresponding EDS-elemental mapping distributions showed the change of C, Al, Cr, Si and N from the 9Cr18 stainless steel substrate to the AlCrSiCN film. There was a continuous change of Cr and Si content from steel to AlCrSiN layer, even from steel to AlCrSiCN layer for Si element, which decreased the mechanics difference between these different layers and enhanced the adhesion force between these transition layers. Fig. 3d showed the HRTEM images of the interface between steel and AlCrSi layer, in which many crystals like FeSi (2 1 0), FeCr (3 3 0) and Fe (2 0 0) were identified as the insets images shown. Especially for the formation of Fe–Si and Fe–Cr bonds, they can dramatically increase the adhesion force between and steel and AlCrSi layer compared with the physical absorption. They were caused by the violent impact on the steel substrate by many high energy ions produced by the HiPIMS method (high ionization rate) and the high bias voltage (−800V).

3.3. Tribological performance and characterizations

Fig. 4a showed the friction coefficient curves within 6000 cycles, and the inset was the schematic diagram of friction process. The AlCrSi/a-C:H and bare-ball tribo-pairs achieved superlubricity (0.0093) and ultra-low coefficient of friction (0.0260) in RH-7% and RH-52%, respectively. And the AlCrSi/a-C:H and a-C:H-ball tribo-pairs all achieved superlubricity both in RH-7% and RH-52%, with the friction coefficient values of 0.0014 and 0.0089. As mentioned above, the low coefficient of friction and high adhesion strength were difficult to reconcile. Fortunately, here, by doping Al, Cr and Si elements in the a-C:H film at the

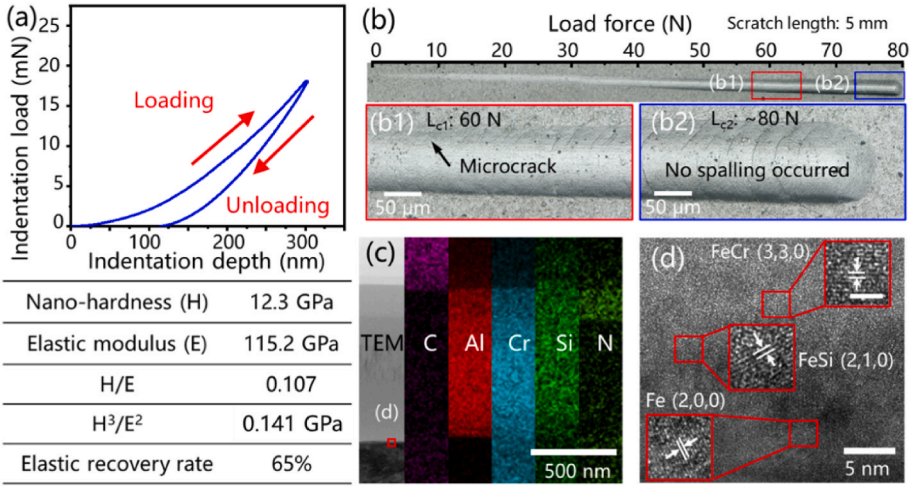

Nano-hardness (H)	12.3 GPa
Elastic modulus (E)	115.2 GPa
H/E	0.107
H^3/E^2	0.141 GPa
Elastic recovery rate	65%

Fig. 3. The mechanical performance of AlCrSi/a-C:H film: (a) nano-indentation force-depth curve and (b) scratch test of AlCrSi/a-C:H film, (c) EDS elemental mapping distributions from the substrate to AlCrSi/a-C:H, and (d) HRTEM images of the interface between substrate and AlCrSi-I layer. (A colour version of this figure can be viewed online.)

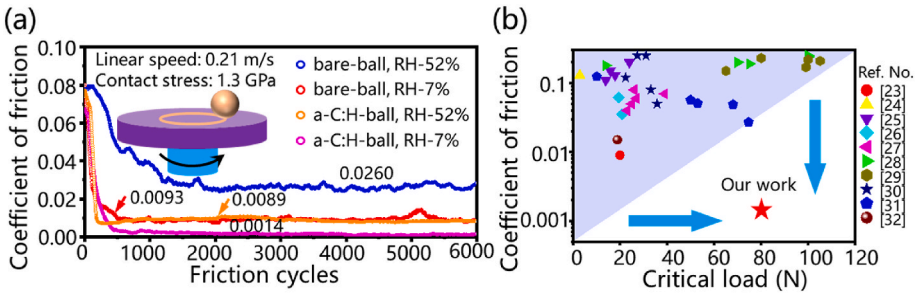

Fig. 4. (a) Friction curves for AlCrSi/a-C:H films against bare-balls and a-C:H-balls in RH-7% and RH-52%, respectively. (b) AlCrSi/a-C:H film with high binding force and superlubricity was obtained. (A colour version of this figure can be viewed online.)

same time, a novel AlCrSi/a-C:H film with high binding force (L_{c2}: ~80 N) and superlubricity (COF 0.0014) was obtained, as the red five-pointed star marked in Fig. 4b, and made its industrial application value greatly improved.

The optical images of tribo-pairs showed the morphology of wear scars on balls and wear tracks on AlCrSi/a-C:H plates (Fig. 5). There was a lot of black debris adhered to the surface of bare-balls and distributed on the edges of wear tracks. And the wear scars on a-C:H-balls presented a smooth surface in the contact area and only little debris was found on the wear tracks of the AlCrSi/a-C:H films. Therefore, in the subsequent sections, to facilitate a more convenient and clear analysis of the composition and structure of the transfer film and investigate its impact on friction, the AlCrSi/a-C:H against bare-balls pair would be the focus of the next Raman, XPS and TEM analyses. Besides, the wear rates of AlCrSi/a-C:H films were calculated according to the wear track sectional profiles obtained by 3D white light interferometry (Fig. S2). It was found that the wear rates of AlCrSi/a-C:H films were both in a very low order of 10^{-8} mm^3/N·m, and the lowest wear rate was 3.33×10^{-8} mm^3/N·m. Obviously, the coefficient of friction acquired in RH-7% was lower than that in RH-52%, because of the low contents of oxygen and water molecules content in RH-7%, and the high content of nitrogen [17,73,74]. So the carbon had a lower chance of bonding with oxygen and water molecules [74], and then AlCrSi/a-C:H films would show better friction performance in RH-7%.

Raman spectra of AlCrSi/a-C:H film against bare-ball tribo-pairs after friction tests were employed to analyze the evolutions of microstructure in films. As shown in Fig. 6a, the D peak intensity of each spectrum after the friction tests showed an increasing trend compared with that of the original film, and the values of I_D/I_G were also increased, which implied the enhancement of sp^2-C clusters and increase of graphitization [56,57]. Besides, the Raman spectra of transfer films were much different from those of deposited AlCrSi/a-C:H films, which were deconvoluted into four peaks at ~1260 cm^{-1} (D1), ~1390 cm^{-1} (D2), ~1500 cm^{-1} (D3) and ~1600 cm^{-1}(Fig. 6a), representing the breath mode of five-membered ring, six-membered ring, seven-membered ring and G peak, respectively [75,76]. The formation of pentatomic and heptatomic rings in the films can relax the internal stress [77]. As reported in Ref. [43,59,60], the promoted graphitization degree was attributed to the incorporation of Al atoms, which could promote the segregation of graphitic carbon, and then formed a low shear strength graphitic layer during the friction process [59,78], thus reduced the friction coefficient.

Elements compositions of AlCrSi/a-C:H film and transfer film after friction test against bare-ball under RH-7% were calculated according to the survey scanning XPS spectra (Fig. S1), and the results showed that the oxygen atoms composition of wear track increased from 13% to 20%, while the carbon atoms composition almost kept the same with original AlCrSi/a-C:H film (Fig. 6b). Moreover, the high resolution XPS spectra of C1s, Al2p, Cr2p, Si2p on wear track after friction test against bare-ball in RH-7% were investigated, as shown in Fig. 6c. According to the C1s peaks, the (C–O and C═O) fractions for wear track was 14.4%, which was reduced by 25% compared with that of original AlCrSi/a-C:H film (19.1%). Meanwhile, the Al, Cr and Si atoms were all mainly existed in the form of oxides, such as Al_2O_3 (98%), Cr_2O_3 (67%) and SiO_2 (97%), based on the Al2p, Cr2p and Si2p peaks splitting results. Synthesize the above analyses results, it was proved that the intense tribo-oxidation reactions occurred, and the oxygen were mainly oxidized with doping elements of Al, Cr and Si rather than C atoms during the sliding process.

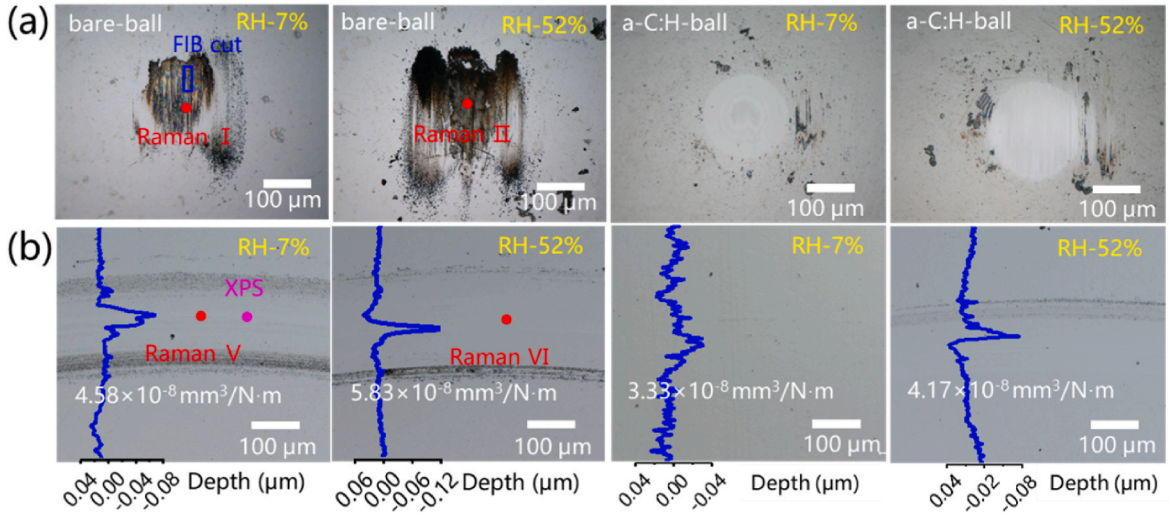

Fig. 5. Optical images of (a) wear scars on balls and (b) corresponding wear tracks with its sectional profiles of AlCrSi/a-C:H films on plates. (A colour version of this figure can be viewed online.)

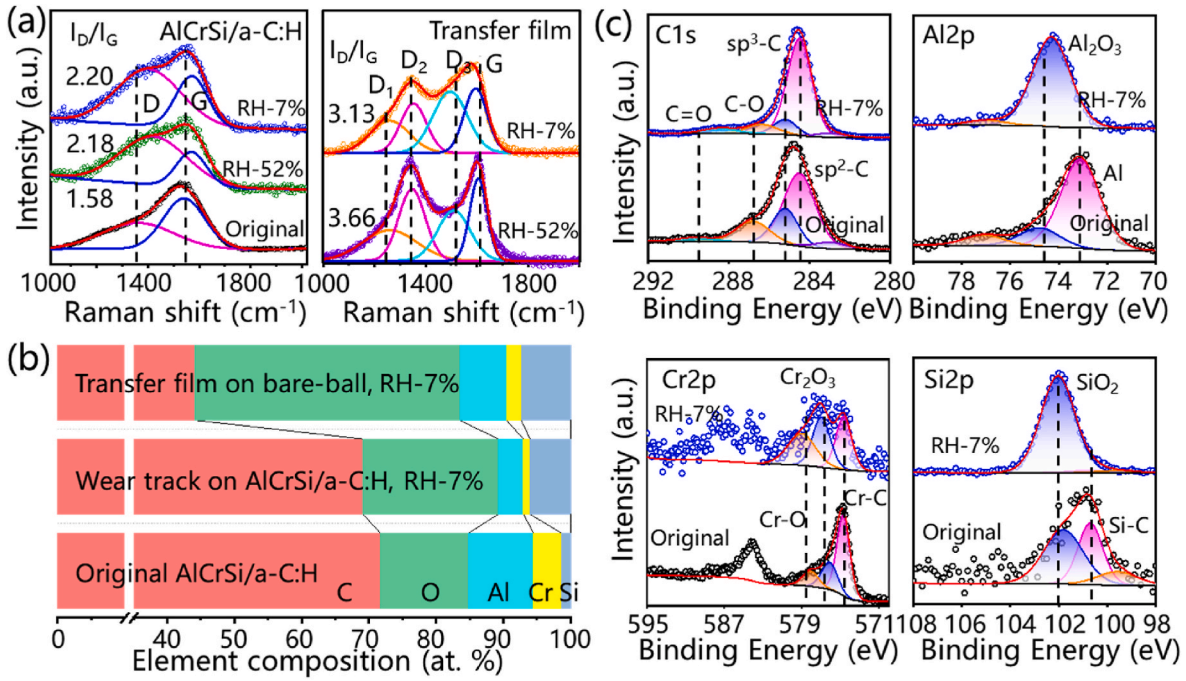

Fig. 6. (a) Raman spectra of tribo-pairs (AlCrSi/a-C:H film against bare ball). (b) Elements composition of the wear track and transfer film after friction tests against bare-ball in RH-7%. (c) High resolution XPS spectra of wear track after friction test against bare-ball in RH-7%.(A colour version of this figure can be viewed online.)

In other words, these tribo-oxidations indirectly protected the carbon from oxidation. Especially, Al atom has the lowest work function value of 4.28 eV compared with other elements of Cr (4.5 eV), Si (4.85 eV) and C (5 eV). As is known, the work function represents an atom's ability to gain or lose electrons, and the smaller the work function, the easier to lose electrons, and the easier to be oxidized. It means that the aluminum atoms have priority to react with oxygen and water molecules compared to carbon, thus protecting the carbon from the effects of oxygen and water molecules to better perform its lubricating role.

3.4. Characterizations of transfer film and wear debris

To further unravel the superlubricity mechanism of AlCrSi/a-C:H films, characterizations of the transfer films and wear debris after friction test against bare-ball were performed. Fig. 7a and b showed the SEM images and EDS-elemental mapping distributions of transfer films formed in RH-7% and RH-52%, respectively. The results suggested that the transfer film in the center of the wear scars mainly contained Al, Cr, Si and O elements, and there was relatively little carbon. In contrast, the wear debris around the wear scars mainly contained C element, and the contents of Al, Cr, Si and O elements were relatively low. Fig. 7c showed the TEM image of cross-sectional morphology of transfer film with a thickness of about 100 nm on bare-ball after friction in RH-7%. The EDS-elemental mapping distributions in transfer film shown in Fig. 7d, the results proved again that the transfer film mainly contained Al, Cr, Si and O elements. And the EDS-elemental line distributions of C, Al, Cr, Si, O, Fe and Pt along the white line showed the carbon and oxygen contents in transfer film were 14.1% and 58.8%, respectively, which were very different from those of XPS (carbon: 44.1%, oxygen: 39.4%) shown in Fig. 6b. Details of detection methods were shown in Fig. S3. Since EDS detected the elemental content of the bulk phase of the transferred film, while XPS detected the elemental content within the top 10 nm of the transferred film's surface, this indicated that the carbon content in the top surface of the transferred film is significantly higher than the bulk carbon content. In other words, there was a carbon-rich layer present on the top surface of the transferred film. And it was the thin carbon-rich layer that played an important role in reducing friction. As Fig. 7e shown, the transfer film mainly consisted of amorphous phase and many fine crystals. Fe_3O_4 crystals (Fig. 7e1) were only observed near the steel ball surface.It proved that the growing transfer film can adhere firmly on the steel ball at the beginning of the friction process, thus avoiding the direct contact between AlCrSi/a-C:H film and steel ball. Besides, Cr_2O_3, Al_2O_3 crystals and oxides amorphous phase were also observed in Fig. 7e2-e4 respectively.

In general, the transfer film was mainly composed of oxides of doped elements and a carbon-rich layer on the top layer which played the main role of lubrication. As a base layer, one side of the oxides adhered to steel ball and the other side to the carbon-rich layer, which avoided the graphite layer contact with steel directly and even be destroyed by the steel. Thus, it ensured that the graphite layer can play a stable role of friction reduction.

As we all known, the abrasive debris was considered as the intermediate products of friction. Part of them participated in forming the transfer film, the others were squeezed to the edge of the wear track and wear scar. Fig. 8a illustrated the EDS-elemental mapping distributions of wear debris collected from the wear track on AlCrSi/a-C:H film after friction against bare-ball in RH-7%, and the results showed that the wear debris mainly consisted of C elements, but the content of Al, Cr, Si and O elements was less, which was consistent with the results mentioned above. Fig. 8b and c showed HRTEM images of wear debris, and it was found that the wear debris mainly consisted of many crystals wrapped in amorphous phase. Fig. 8b1-b2 confirmed that the crystals were Al_2O_3 (311) with a lattice spacing of 0.238 nm and Al_2O_3 (400) with a lattice spacing of 0.203 nm [79,80]. And two or three graphite layers and the ordered graphite-like structures were also observed at the edge of the amorphous phase in Fig. 8c1-c2. The presence of these carbon layers once again proved the existence of friction graphitization, and it was the low shear force between the graphite layers that contributed to the superlubricity. Meanwhile, this specific structure: oxides crystals and amorphous carbon particles wrapped in graphite layers or ordered graphite-like structure avoided the direct participation of oxides in friction, thereby ensuring the stable realization of robust superlubricity.

In order to further explore the formation process of transfer film and figure out where the carbon went, a series of friction tests during

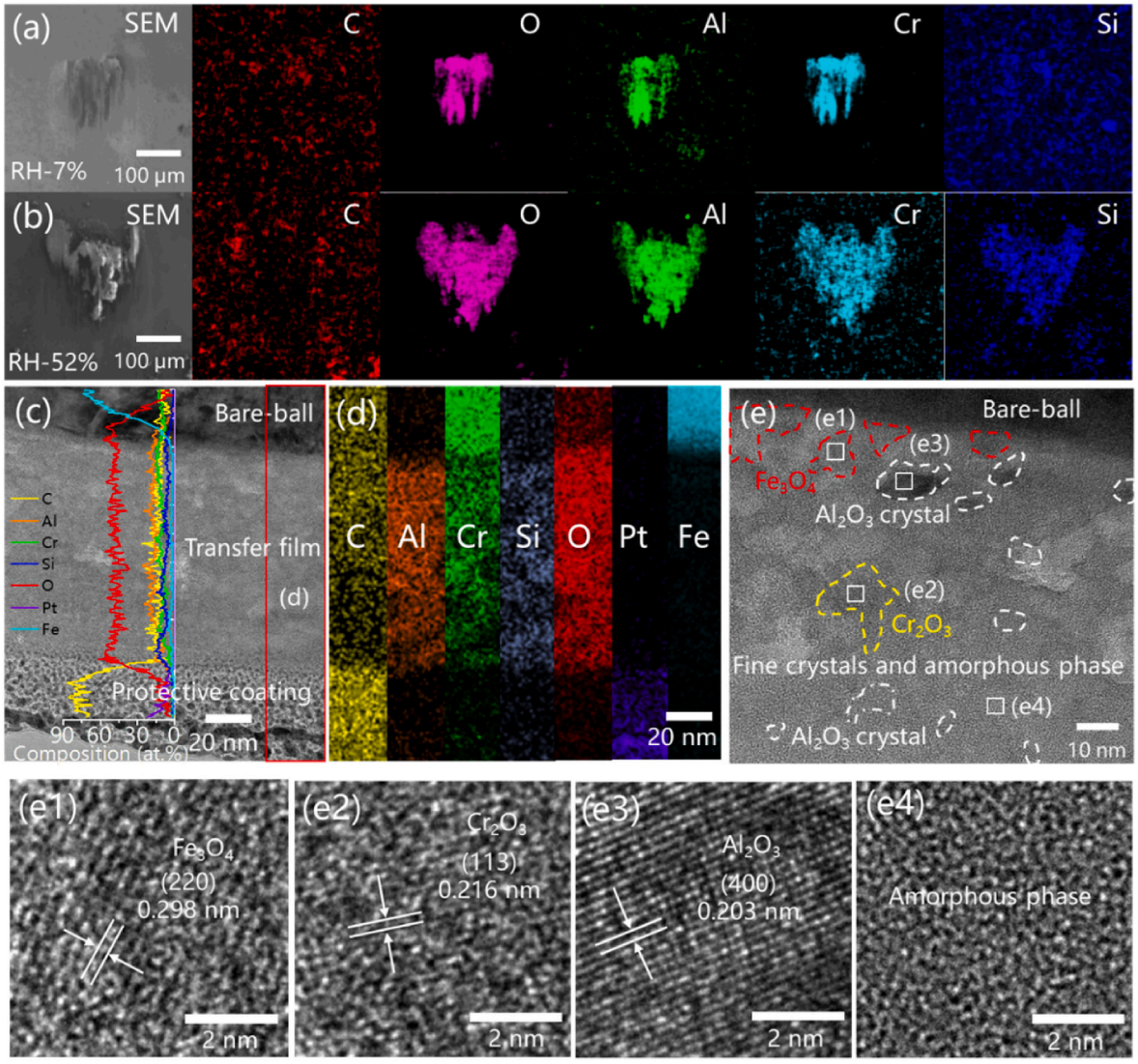

Fig. 7. Characterizations of transfer film on bare-ball: SEM images and EDS-elemental mapping distributions of transfer films formed in (a) RH-7% and (b) RH-52%. (c) TEM cross sectional image of transfer film formed in RH-7% with its EDS-elemental line and (d) mapping distributions. (e) HRTEM images of transfer film formed in RH-7%, and (e1)-(e3) crystal structures, (e4) amorphous phase. (A colour version of this figure can be viewed online.)

running-in stages were conducted in RH-7%, as seen in Fig. S4. According to the detail analyses described in the supplementary information, as friction progresses, the graphitized carbon layers used for friction reduction would continuously be expelled from the frictional area, forming wear debris outside the contact region. This left most of the oxides adhered to the steel ball surface, forming a transfer film and resulting in a reduction in carbon content within the transfer film.

Under high humidity (RH-52%), the AlCrSi/a-C:H film against an a-C:H-ball tribo-pairs also achieved superlubricity. According to the characterizations shown in Fig. S5 and the analyses in the supplementary information, like the AlCrSi/a-C:H film and bare-ball pair, when AlCrSi/a-C:H film rubbed against an a-C:H-ball, the promoted graphitization and the preferential oxidation of doping elements were also occurred. However, achieving superlubricity during friction with an a-C:H-ball in high humidity conditions (RH-52%) should also be attributed to two additional factors: Firstly, when carbon films rubbed against each other, both sides of the sliding pair provided ample amounts of doping elements capable of preferentially combining with oxygen, further enhancing protection for the graphite layer. Secondly, oxides formed from doping elements did not adhere to either side of the sliding pair but were expelled from the frictional area along with the carbon layer as part of wear debris. This allowed both sides of the frictional area to offer sufficient carbon layers for reducing friction and further promoting superlubricity.

3.5. *Modelling of superlubricity promoted by doping elements*

Based on these characterizations results, the mechanisms governing the superlubricity behaviors of AlCrSi/a-C:H film were proposed in Fig. 9. Al, Cr and Si doping elements dominated two essential processes in the whole friction: graphitization and tribo-oxidation reaction. On the one hand, the doping element of Al can promote the graphitization [43,59,60], which can be confirmed by Raman results and the graphite layers formed on the outmost surface of transfer film and the formation of graphite layers. On the other hand, the doping elements of Al, Cr and Si had a stronger ability to react with oxygen rather than carbon, which would help to reduce the oxidation degree of the graphite layers, and ensure that the graphite layer played a good role in reducing friction [59,81,82]. At the same time, the oxides produced by the tribo-oxidation reaction would also be wrapped by the graphite layers avoiding the direct participation of oxides in friction, further ensuring the good friction performance. Therefore, the interaction and mutual promotion

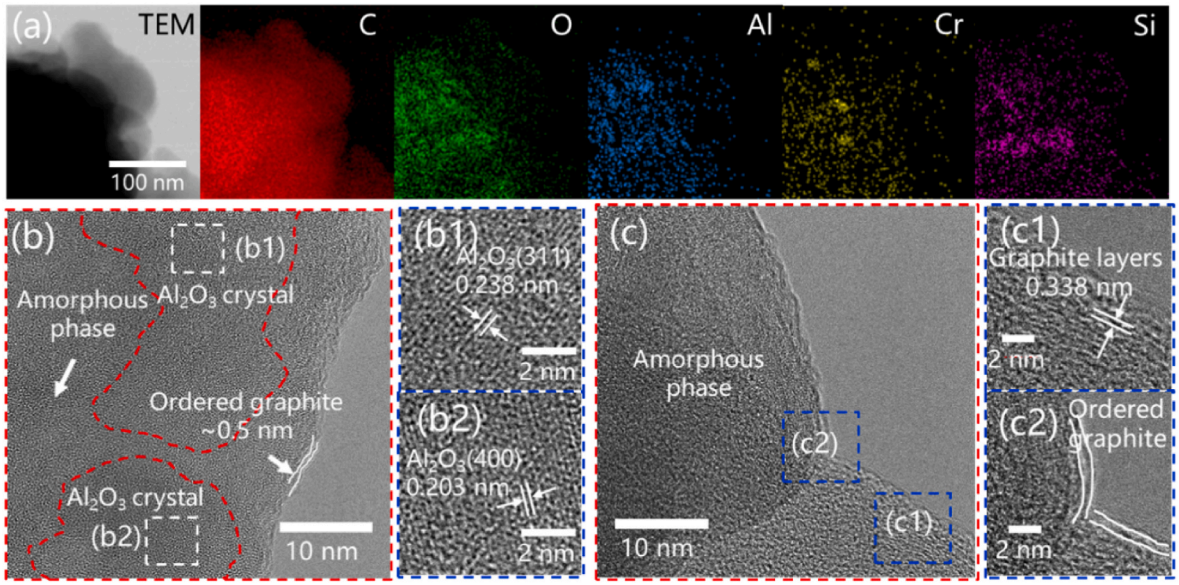

Fig. 8. Characterizations of wear debris after sliding against bare-balls in RH-7%: (a) TEM image and EDS-elemental mapping distributions of wear debris. HRTEM images of the wear debris consisting of (b) Al_2O_3 crystals wrapped in amorphous carbon phase and the ordered graphite structures and (c) the graphite layers. HRTEM images of (b1, b2) Al_2O_3 crystals, (c1) graphite layers and (c2) ordered graphite structures. (A colour version of this figure can be viewed online.)

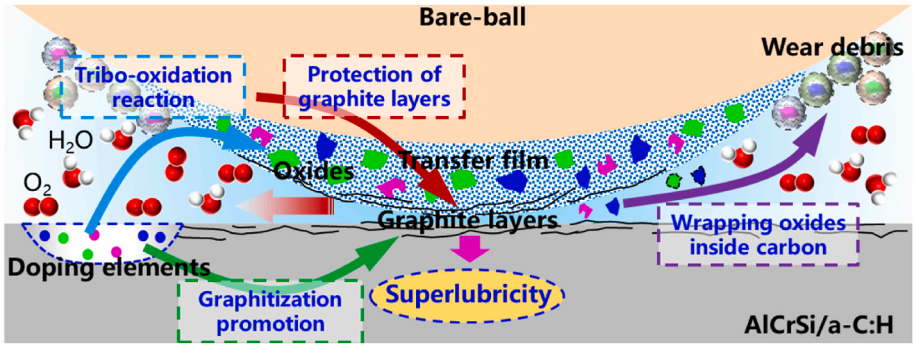

Fig. 9. Superlubricity mechanism schematic diagram of AlCrSi/a-C:H film. (A colour version of this figure can be viewed online.)

between graphitization and tribo-oxidation reaction promoted by doping elements resulted in the realization of stable superlubricity.

4. Conclusion

In this work, a kind of multi-doping AlCrSi/a-C:H films with both high adhesion strength (L_{C2}: ~80 N) and superlubricity (COF 0.0014) were prepared using HiPIMS method. The friction results showed that AlCrSi/a-C:H film achieved superlubricity both in RH-52% and RH-7% conditions. A series of characterizations suggested that doping elements, especially for Al element, contributed to the graphitization and oxidation. Meanwhile, the preferential oxidation of Al, Cr and Si elements can reduce the oxidation degree of carbon, and the graphite layers produced by graphitization can wrap the oxides to prevent their adverse effects on friction. It was the synergistic effects of the graphitization and oxidation that led to the superlubricity. Hence, the AlCrSi/a-C:H film with strong adhesion and excellent friction performance is expected to be widely used in industrial field.

CRediT authorship contribution statement

Quansheng Ma: Data curation, Investigation, Writing – original draft. **Yongqiang Fu:** Writing – review & editing. **Yi Xu:** Resources, Writing – review & editing. **Tianbao Ma:** Supervision, Conceptualization, Writing – review & editing.

Declaration of competing interest

The authors declare that they have no known competing financial interests or personal relationships that could have appeared to influence the work reported in this paper.

Acknowledgments

This work was supported by National Natural Science Foundation of China (Grant No. 52225502, 52301068, 52205204), National Key R&D Program of China (No:2021YFB3500100).

Appendix A. Supplementary data

Supplementary data to this article can be found online at https://doi.org/10.1016/j.carbon.2023.118424.

References

[1] W. Cui, K. Raza, Z. Zhao, C. Yu, L. Tao, W. Zhao, W. Chen, S. Peng, Q. Xu, L. Ma, Role of transfer film formation on the tribological properties of polymeric composite materials and spherical plain bearing at low temperatures, Tribol. Int. 152 (2020), 106569.

[2] K.C. Mutyala, Y.A. Wu, A. Erdemir, A.V. Sumant, Graphene-MoS_2 ensembles to reduce friction and wear in DLC-Steel contacts, Carbon 146 (2019) 524–527.
[3] M. Xu, Z. Wang, L. Guo, L. Tao, T. Ma, T. Wang, Q. Wang, Tribological properties of PTFE-based fabric composites at cryogenic temperature, Friction (2023) 1–13.
[4] Y. Meng, J. Xu, L. Ma, Z. Jin, B. Prakash, T. Ma, W. Wang, A review of advances in tribology in 2020–2021, Friction 10 (2022) 1443–1595.
[5] W. Zhai, N. Srikanth, L.B. Kong, K. Zhou, Carbon nanomaterials in tribology, Carbon 119 (2017) 150–171.
[6] Z. Gong, J. Shi, B. Zhang, J. Zhang, Graphene nano scrolls responding to superlow friction of amorphous carbon, Carbon 116 (2017) 310–317.
[7] X. Chen, J. Li, Superlubricity of carbon nanostructures, Carbon 158 (2020) 1–23.
[8] J. Wang, Z. Cao, F. Pan, F. Wang, A. Liang, J. Zhang, Tuning of the microstructure, mechanical and tribological properties of a-C: H films by bias voltage of high frequency unipolar pulse, Appl. Surf. Sci. 356 (2015) 695–700.
[9] X. Liu, J. Hao, Y. Xie, Silicon and aluminum doping effects on the microstructure and properties of polymeric amorphous carbon films, Appl. Surf. Sci. 379 (2016) 358–366.
[10] A. Erdemir, O. Eryilmaz, I. Nilufer, G. Fenske, Effect of source gas chemistry on tribological performance of diamond-like carbon films, Diam. Relat. Mater. 9 (2000) 632–637.
[11] A. Erdemir, Genesis of superlow friction and wear in diamondlike carbon films, Tribol. Int. 37 (2004) 1005–1012.
[12] P. Wang, M. Hirose, Y. Suzuki, K. Adachi, Carbon tribo-layer for super-low friction of amorphous carbon nitride coatings in inert gas environments, Surf. Coating. Technol. 221 (2013) 163–172.
[13] A. Erdemir, O. Eryilmaz, S. Kim, Effect of tribochemistry on lubricity of DLC films in hydrogen, Surf. Coating. Technol. 257 (2014) 241–246.
[14] X. Chen, C. Zhang, T. Kato, X.-a. Yang, S. Wu, R. Wang, M. Nosaka, J. Luo, Evolution of tribo-induced interfacial nanostructures governing superlubricity in a-C: H and a-C: H: Si films, Nat. Commun. 8 (2017) 1–13.
[15] P. Manimunda, A. Al-Azizi, S.H. Kim, R.R. Chromik, Shear-induced structural changes and origin of ultralow friction of hydrogenated diamond-like carbon (DLC) in dry environment, ACS Appl. Mater. Interfaces 9 (2017) 16704–16714.
[16] Y. Wang, K. Gao, B. Zhang, Q. Wang, J. Zhang, Structure effects of sp^2-rich carbon films under super-low friction contact, Carbon 137 (2018) 49–56.
[17] C. Wang, B. Li, X. Ling, J. Zhang, Superlubricity of hydrogenated carbon films in a nitrogen gas environment: adsorption and electronic interactions at the sliding interface, RSC Adv. 7 (2017) 3025–3034.
[18] A. Erdemir, O. Eryilmaz, Achieving superlubricity in DLC films by controlling bulk, surface, and tribochemistry, Friction 2 (2014) 140–155.
[19] Z.-J. Wang, T.-B. Ma, Y.-Z. Hu, L. Xu, H. Wang, Energy dissipation of atomic-scale friction based on one-dimensional Prandtl-Tomlinson model, Friction 3 (2015) 170–182.
[20] Y. Liu, L. Chen, B. Zhang, Z. Cao, P. Shi, Y. Peng, N. Zhou, J. Zhang, L. Qian, Key role of transfer layer in load dependence of friction on hydrogenated diamond-like carbon films in humid air and vacuum, Materials 12 (2019) 1550.
[21] J. Wang, X. Li, G. Wu, Z. Lu, G. Zhang, Q. Xue, Origin of low friction for amorphous carbon films with different hydrogen content in nitrogen atmosphere, Tribol. Int. 140 (2019), 105853.
[22] X. Liu, P. Gong, H. Hu, M. Zhao, K. Zhang, H. Zhou, Study on the tribological properties of PVD polymer-like carbon films in air/vacuum/N_2 and cycling environments, Surf. Coating. Technol. 406 (2021), 126677.
[23] L. Sun, K. Gao, Q. Jia, C. Bai, B. Zhang, X. Tan, J. Zhang, Grown of superlubricity a-C: H/MoS_2 film on 9Cr18Mo steel for industrial application, Diam. Relat. Mater. 117 (2021), 108479.
[24] A. Yetim, H. Kovacı, A. Kasapoğlu, Y. Bozkurt, A. Çelik, Influences of Ti, Al and V metal doping on the structural, mechanical and tribological properties of DLC films, Diam. Relat. Mater. 120 (2021), 108639.
[25] J. Wang, J. Ma, W. Huang, L. Wang, H. He, C. Liu, The investigation of the structures and tribological properties of F-DLC coatings deposited on Ti-6Al-4V alloys, Surf. Coating. Technol. 316 (2017) 22–29.
[26] J. Wang, X. Cao, Z. Lu, G. Zhang, Q. Xue, The improved mechanical and tribological properties of amorphous carbon film by doping boron carbide, Ceram. Int. 46 (2020) 9878–9884.
[27] A. Li, X. Li, Y. Wang, Z. Lu, Y. Wang, G. Zhang, Z. Wu, Investigation of mechanical and tribological properties of super-thick DLC films with different modulation ratios prepared by PECVD, Mater. Res. Express 6 (2019), 086433.
[28] P. Jing, D. Ma, Y. Gong, X. Luo, Y. Zhang, Y. Weng, Y. Leng, Influence of Ag doping on the microstructure, mechanical properties, and adhesion stability of diamond-like carbon films, Surf. Coating. Technol. 405 (2021), 126542.
[29] Z. Fu, C. Wang, W. Zhang, W. Wang, W. Yue, X. Yu, Z. Peng, S. Lin, M. Dai, Influence of W content on tribological performance of W-doped diamond-like carbon coatings under dry friction and polyalpha olefin lubrication conditions, Mater. Des. 51 (2013) 775–779.
[30] Y. Zhou, L. Li, W. Shao, Z. Chen, S. Wang, X. Xing, Q. Yang, Mechanical and tribological behaviors of Ti-DLC films deposited on 304 stainless steel: exploration with Ti doping from micro to macro, Diam. Relat. Mater. 107 (2020), 107870.
[31] W. Xu, K. Zhou, S. Lin, M. Dai, Q. Shi, C. Wei, Structural properties of hydrogenated Al-doped diamond-like carbon films fabricated by a hybrid plasma system, Diam. Relat. Mater. 87 (2018) 177–185.
[32] Y. Zhao, P. Ju, H. Liu, L. Pei, L. Ji, H. Li, D. Xue, H. Zhou, J. Chen, A strategy to construct long-range fullerene-like nanostructure in amorphous carbon film with improved toughness and carrying capacity, J. Phys. Appl. Phys. 53 (2020), 335205.
[33] Y. Xiao, W. Shi, Z. Han, J. Luo, L. Xu, Residual stress and its effect on failure in a DLC coating on a steel substrate with rough surfaces, Diam. Relat. Mater. 66 (2016) 23–35.
[34] X. Pang, L. Shi, P. Wang, Y. Xia, W. Liu, Effects of Al incorporation on the mechanical and tribological properties of Ti-doped a-C:H films deposited by magnetron sputtering, Curr. Appl. Phys. 11 (2011) 771–775.
[35] J. Pu, G. Zhang, S. Wan, R. Zhang, Synthesis and characterization of low-friction Al-DLC films with high hardness and low stress, J. Compos. Mater. 49 (2015) 199–207.
[36] J. Pu, D. He, L. Wang, Effects of WC phase contents on the microstructure, mechanical properties and tribological behaviors of WC/a-C superlattice coatings, Appl. Surf. Sci. 357 (2015) 2039–2047.
[37] D. Zhang, P. Yi, L. Peng, X. Lai, J. Pu, Amorphous carbon films doped with silver and chromium to achieve ultra-low interfacial electrical resistance and long-term durability in the application of proton exchange membrane fuel cells, Carbon 145 (2019) 333–344.
[38] D. Martínez-Martínez, C. López-Cartes, A. Fernández, J. Sánchez-López, Influence of the microstructure on the mechanical and tribological behavior of TiC/a-C nanocomposite coatings, Thin Solid Films 517 (2009) 1662–1671.
[39] P. Zhang, B. Tay, C. Sun, S.P. Lau, Microstructure and mechanical properties of nanocomposite amorphous carbon films, J. Vac. Sci. Technol. A: Vacuum, Surfaces, and Films 20 (2002) 1390–1394.
[40] S. Gayathri, N. Kumar, R. Krishnan, T. Ravindran, S. Dash, A. Tyagi, M. Sridharan, Influence of Cr content on the micro-structural and tribological properties of PLD grown nanocomposite DLC-Cr thin films, Mater. Chem. Phys. 167 (2015) 194–200.
[41] Z. Wu, X. Tian, G. Gui, C. Gong, S. Yang, P.K. Chu, Microstructure and surface properties of chromium-doped diamond-like carbon thin films fabricated by high power pulsed magnetron sputtering, Appl. Surf. Sci. 276 (2013) 31–36.
[42] J. Sánchez-López, D. Martínez-Martínez, C. López-Cartes, A. Fernández, Tribological behaviour of titanium carbide/amorphous carbon nanocomposite coatings: from macro to the micro-scale, Surf. Coating. Technol. 202 (2008) 4011–4018.
[43] W. Dai, A. Wang, Deposition and properties of Al-containing diamond-like carbon films by a hybrid ion beam sources, J. Alloys Compd. 509 (2011) 4626–4631.
[44] C. Zou, H. Wang, L. Feng, S. Xue, Effects of Cr concentrations on the microstructure, hardness, and temperature-dependent tribological properties of Cr-DLC coatings, Appl. Surf. Sci. 286 (2013) 137–141.
[45] L. Qiang, K. Gao, L. Zhang, J. Wang, B. Zhang, J. Zhang, Further improving the mechanical and tribological properties of low content Ti-doped DLC film by W incorporating, Appl. Surf. Sci. 353 (2015) 522–529.
[46] Y. Zhou, P. Guo, L. Sun, L. Liu, X. Xu, W. Li, X. Li, K.-R. Lee, A. Wang, Microstructure and property evolution of diamond-like carbon films co-doped by Al and Ti with different ratios, Surf. Coating. Technol. 361 (2019) 83–90.
[47] G. Zhang, P. Yan, P. Wang, Y. Chen, J. Zhang, The preparation and mechanical properties of Al-containing a-C:H thin films, J. Phys. Appl. Phys. 40 (2007) 6748.
[48] X. Chen, T. Kato, M. Kawaguchi, M. Nosaka, J. Choi, Structural and environmental dependence of superlow friction in ion vapour-deposited a-C:H:Si films for solid lubrication application, J. Phys. Appl. Phys. 46 (2013), 255304.
[49] X. Chen, T. Kato, M. Nosaka, Origin of superlubricity in a-C:H:Si films: a relation to film bonding structure and environmental molecular characteristic, ACS Appl. Mater. Interfaces 6 (2014) 13389–13405.
[50] X. Chen, X. Yin, W. Qi, C. Zhang, J. Choi, S. Wu, R. Wang, J. Luo, Atomic-scale insights into the interfacial instability of superlubricity in hydrogenated amorphous carbon films, Sci. Adv. 6 (2020) 1272.
[51] X. Liu, J. Yang, J. Hao, J. Zheng, Q. Gong, W. Liu, Microstructure, mechanical and tribological properties of Si and Al co-doped hydrogenated amorphous carbon films deposited at various bias voltages, Surf. Coating. Technol. 206 (2012) 4119–4125.
[52] K. Sarakinos, J. Alami, S. Konstantinidis, High power pulsed magnetron sputtering: a review on scientific and engineering state of the art, Surf. Coating. Technol. 204 (2010) 1661–1684.
[53] J. Alami, K. Sarakinos, F. Uslu, M. Wuttig, On the relationship between the peak target current and the morphology of chromium nitride thin films deposited by reactive high power pulsed magnetron sputtering, J. Phys. Appl. Phys. 42 (2008), 015304.
[54] J. Archard, Contact and rubbing of flat surfaces, J. Appl. Phys. 24 (1953) 981–988.
[55] C. Casiraghi, A. Ferrari, J. Robertson, Raman spectroscopy of hydrogenated amorphous carbons, Phys. Rev. B 72 (2005), 085401.
[56] A.C. Ferrari, J. Robertson, Resonant Raman spectroscopy of disordered, amorphous, and diamondlike carbon, Phys. Rev. B 64 (2001), 075414.
[57] G. Irmer, A. Dorner-Reisel, Micro-Raman studies on DLC coatings, Adv. Eng. Mater. 7 (2005) 694–705.
[58] J. Wang, Z. Cao, F. Pan, F. Wang, A. Liang, J. Zhang, Tuning of the microstructure, mechanical and tribological properties of a-C:H films by bias voltage of high frequency unipolar pulse, Appl. Surf. Sci. 356 (2015) 695–700.
[59] C. Kong, P. Guo, L. Sun, Y. Zhou, Y. Liang, X. Li, P. Ke, K.-R. Lee, A. Wang, Tribological mechanism of diamond-like carbon films induced by Ti/Al co-doping, Surf. Coating. Technol. 342 (2018) 167–177.
[60] X. Liu, J. Hao, J. Yang, J. Zheng, Y. Liang, W. Liu, Preparation of superior lubricious amorphous carbon films co-doped by silicon and aluminum, J. Appl. Phys. 110 (2011), 053507.
[61] K. Wang, B. Yang, B. Zhang, C. Bai, Z. Mou, K. Gao, G. Yushkov, E. Oks, Modification of a-C:H films via nitrogen and silicon doping: the way to the superlubricity in moisture atmosphere, Diam. Relat. Mater. 107 (2020), 107873.
[62] J. Hao, T. Xu, W. Liu, Effect of deposition pressure on microstructure and properties of hydrogenated carbon nitride films prepared by DC-RF-PECVD, J. Non-Cryst. Solids 351 (2005) 3671–3676.
[63] A. Singha, A. Ghosh, A. Roy, N.R. Ray, Quantitative analysis of hydrogenated diamondlike carbon films by visible Raman spectroscopy, J. Appl. Phys. 100 (2006), 044910.

[64] W. Dai, J. Liu, D. Geng, P. Guo, J. Zheng, Q. Wang, Microstructure and property of diamond-like carbon films with Al and Cr co-doping deposited using a hybrid beams system, Appl. Surf. Sci. 388 (2016) 503–509.
[65] V. Singh, J. Jiang, E. Meletis, Cr-diamondlike carbon nanocomposite films: synthesis, characterization and properties, Thin Solid Films 489 (2005) 150–158.
[66] S. Yi, X. Chen, J. Li, Y. Liu, S. Ding, J. Luo, Macroscale superlubricity of Si-doped diamond-like carbon film enabled by graphene oxide as additives, Carbon 176 (2021) 358–366.
[67] K.L. Johnson, K.L. Johnson, Contact Mechanics, Cambridge university press, 1987.
[68] W. Dai, X. Gao, J. Liu, Q. Wang, Microstructure, mechanical property and thermal stability of diamond-like carbon coatings with Al, Cr and Si multi-doping, Diam. Relat. Mater. 70 (2016) 98–104.
[69] W. Dai, P. Ke, A. Wang, Influence of bias voltage on microstructure and properties of Al-containing diamond-like carbon films deposited by a hybrid ion beam system, Surf. Coating. Technol. 229 (2013) 217–221.
[70] A. C-05, Standard Test Method for Adhesion Strength and Mechanical Failure Modes of Ceramic Coatings by Quantitative Single Point Scratch Testing, 2005.
[71] T. Hao, J. Du, G. Su, P. Zhang, Y. Sun, J. Zhang, Mechanical and cutting performance of cemented carbide tools with Cr/x/DLC composite coatings, Int. J. Adv. Des. Manuf. Technol. 106 (2020) 5241–5254.
[72] B. Zhou, B. Xu, Y. Xu, S. Yu, Y. Wu, Y. Wu, Z. Liu, Selective bonding effect on microstructure and mechanical properties of (Al, N)-DLC composite films by ion beam-assisted cathode arc evaporation, Appl. Phys. A 125 (2019) 1–15.
[73] L. Ji, H. Li, F. Zhao, W. Quan, J. Chen, H. Zhou, Effects of environmental molecular characteristics and gas–surface interaction on friction behaviour of diamond-like carbon films, J. Phys. Appl. Phys. 42 (2009), 135301.
[74] D. Zhu, H. Li, L. Ji, H. Zhou, J. Chen, Tribochemistry of superlubricating amorphous carbon films, Chem. Commun. 57 (2021) 11776–11786.
[75] T.S. Yang, J.Y. Lai, C.L. Cheng, M.S. Wong, Growth of faceted, ballas-like and nanocrystalline diamond films deposited in CH_4/H_2/Ar MPCVD, Diam. Relat. Mater. 10 (2001) 2161–2166.
[76] Q. Wang, C. Wang, Z. Wang, J. Zhang, D. He, Fullerene nanostructure-induced excellent mechanical properties in hydrogenated amorphous carbon, Appl. Phys. Lett. 91 (2007), 141902.
[77] Y. Wang, Y. Wang, X. Zhang, J. Shi, K. Gao, B. Zhang, J. Zhang, Hydrogenated amorphous carbon films on steel balls and Si substrates: nanostructural evolutions and their trigging tribological behaviors, Appl. Surf. Sci. 420 (2017) 586–593.
[78] S. Zhou, L. Wang, Z. Lu, Q. Ding, S. Wang, R.J. Wood, Q. Xue, Tailoring microstructure and phase segregation for low friction carbon-based nanocomposite coatings, J. Mater. Chem. 22 (2012) 15782–15792.
[79] X. Rong, X. Zhang, D. Zhao, C. He, C. Shi, E. Liu, N. Zhao, In-situ Al_2O_3-Al interface contribution towards the strength-ductility synergy of Al-CuO composite fabricated by solid-state reactive sintering, Scripta Mater. 198 (2021), 113825.
[80] Y. Shan, B. Pu, E. Liu, C. Shi, C. He, N. Zhao, In-situ synthesis of CNTs@ Al_2O_3 wrapped structure in aluminum matrix composites with balanced strength and toughness, Mater. Sci. Eng., A 797 (2020), 140058.
[81] H. Pollock, Surface Forces and Adhesion, Fundamentals of Friction: Macroscopic and Microscopic Processes, Springer, 1992, pp. 77–94.
[82] L. Ji, H. Li, F. Zhao, W. Quan, J. Chen, H. Zhou, Atomic oxygen resistant behaviors of Mo/diamond-like carbon nanocomposite lubricating films, Appl. Surf. Sci. 255 (2009) 4180–4184.